NeuroImage xxx (2013) xxx–xxx

Contents lists available at ScienceDirect

NeuroImage

journal homepage: www.elsevier.com/locate/ynimg

The structural–functional connectome and the default mode network of the human brain

Andreas Horn [a,b,*], Dirk Ostwald [a], Marco Reisert [c], Felix Blankenburg [a,d]

[a] Center for Adaptive Rationality (ARC), Max Planck Institute for Human Development, Berlin, Germany
[b] Department of Neurology, Charité, University Medicine Berlin, Berlin, Germany
[c] Department of Radiology, Medical Physics, University Hospital Freiburg, Germany
[d] Dahlem Institute for Neuroimaging of Emotion, Freie Universität Berlin, Berlin, Germany

ARTICLE INFO

Article history:
Accepted 25 September 2013
Available online xxxx

Keywords:
Connectome
Structure–function relationship
Functional magnetic resonance imaging (fMRI)
Diffusion tensor imaging (DTI)
Resting-state fMRI
Default mode network (DMN)

ABSTRACT

An emerging field of human brain imaging deals with the characterization of the connectome, a comprehensive global description of structural and functional connectivity within the human brain. However, the question of how functional and structural connectivity are related has not been fully answered yet. Here, we used different methods to estimate the connectivity between each voxel of the cerebral cortex based on functional magnetic resonance imaging (fMRI) and diffusion tensor imaging (DTI) data in order to obtain observer-independent functional–structural connectomes of the human brain. Probabilistic fiber-tracking and a novel global fiber-tracking technique were used to measure structural connectivity whereas for functional connectivity, full and partial correlations between each voxel pair's fMRI-timecourses were calculated. For every voxel, two vectors consisting of functional and structural connectivity estimates to all other voxels in the cortex were correlated with each other. In this way, voxels structurally and functionally connected to similar regions within the rest of the brain could be identified. Areas forming parts of the 'default mode network' (DMN) showed the highest agreement of structure–function connectivity. Bilateral precuneal and inferior parietal regions were found using all applied techniques, whereas the global tracking algorithm additionally revealed bilateral medial prefrontal cortices and early visual areas. There were no significant differences between the results obtained from full and partial correlations. Our data suggests that the DMN is the functional brain network, which uses the most direct structural connections. Thus, the anatomical profile of the brain seems to shape its functional repertoire and the computation of the whole-brain functional–structural connectome appears to be a valuable method to characterize global brain connectivity within and between populations.

Introduction

The analysis of structural and functional connectivity between different regions of the brain provides profound insights into its underlying organization. Thus, both kinds of brain connectivity have been extensively studied over the last years, leading to the concept of the connectome, which was first defined for structural connectivity as a 'comprehensive structural description of the network of elements and connections forming the human brain' (Sporns et al., 2005). Later, the concept was extended to include functional connectivity, i.e. the functional connectome (Biswal et al., 2010; Zuo et al., 2011). However, only few studies have focused on the relationship between structural and functional brain connectivity (for reviews see Bassett and Bullmore, 2009; Damoiseaux and Greicius, 2009; Honey et al., 2010; Rykhlevskaia et al., 2008; Sporns, 2011).

Koch et al. (Koch et al., 2002) were first to combine two MRI-imaging techniques to directly study the interplay between structure and function of the human brain. Using diffusion tensor imaging (DTI) and resting-state functional magnetic resonance imaging (fMRI) they provided evidence that fMRI signal correlations reflect the presence of direct and indirect anatomical pathways. Findings from 23 pairs of voxels each situated in two adjacent gyri on a single axial slice were reported. All time courses from structurally connected voxels were also correlated functionally. In some cases, however, functional connectivity was also found in the absence of robust structural connectivity. Building up on this initial point-to-point analysis, a study by (Greicius et al., 2009) found structural connectivity between functionally connected parts of the default mode network (DMN), a set of regions typically active at rest (Buckner et al., 2008; Raichle et al., 2001; Shulman et al., 1997). The precuneus/retrosplenial cortex was found to be structurally connected with bilateral medial temporal lobes (MTL) and the medial prefrontal cortex (MPFC). Tracts starting from the medial prefrontal cortex (MPFC) contacted the posterior cingulate cortex (PCC).

A similar study extended these qualitative findings to a quantitative level (van den Heuvel et al., 2008). Partial correlations between the PCC

* Corresponding author at: Center for Adaptive Rationality (ARC), Max Planck Institute for Human Development, Lentzeallee 94, 14195 Berlin, Germany. Fax: +49 30 824 06 490.
E-mail address: andreas.horn@mpib-berlin.mpg.de (A. Horn).

1053-8119/$ – see front matter © 2013 Elsevier Inc. All rights reserved.
http://dx.doi.org/10.1016/j.neuroimage.2013.09.069

and the MPFC (regressing out 15 other clusters within the DMN and other resting-state networks) accounted for functional connectivity strength, whereas mean fractional anisotropy values of the cingulum were used as a measure for structural connectivity strength. The two measures of connectivity strength correlated between subjects, which suggests that a strong structural basis leads to strong functional couplings between regions.

A limitation of region-to-region connectivity measurements, as applied in the studies above, is that regions of interest must be manually selected, possibly introducing selection bias (Damoiseaux and Greicius, 2009). To avoid this, data-driven approaches such as independent component analysis (ICA) have become increasingly common, allowing for the analysis of functional connectivity across the whole brain. A study by (Segall et al., 2012) and colleagues simultaneously applied ICA on functional time courses and gray matter density values (Xu et al., 2009) to analyze the global structure–function relationship. High spatial overlap between functional and structural ICA components was found. However, in the ICA framework, the number of independent components has to be defined typically a priori and the technique cannot be applied easily to anatomical white-matter connectivity.

A different approach that allows for analyzing whole-brain connectivity without a manual definition of regions of interest is to measure connectivity between each pair of voxels within the gray matter. To the best of our knowledge, only few studies have used such an approach and only two have focused on the relationship between structure and function in a voxel-wise (Skudlarski et al., 2008) or more coarsely parcellated fashion (Honey et al., 2009).

In the study by Honey et al., the brain was initially divided into 66 regions based on landmarks using FreeSurfer (Fischl et al., 2004). These regions were then further subdivided into 998 areas of approximately equal size. Functional connectivity was measured by correlating the mean fMRI signals of each area. The number of fiber tracts connecting regions was used as a measure or their structural connectivity strength. It was found that both indices of connectivity strength correlated between regions. However, as shown in the studies by Koch et al. and Greicius et al., functional connectivity was also found between regions that were not directly connected by anatomical tracts. In the study by Skudlarski and colleagues, the agreement between structure and function was analyzed in a voxel-wise fashion. Thereby, functional and structural connectivity between each of 5000 downsampled isotropic 4 mm voxels within the gray matter was compared. Strongest correlations between functional and structural connectivity were found in highly connected regions such as the thalamus, precuneus and anterior cingulate.

Based on the work by Skudlarski et al., in the current study we estimated structural and functional connectivity at high spatial resolution between each pair of 40,000 voxels, defined by a group-template that best represented the mean anatomy of all participants of the study. For each voxel within the cortex, structural and functional connectivity to all other voxels was estimated. Thus, connectivity vectors that accounted for different connectivity estimates of a certain voxel to the rest of the brain were established. In a second step, these were correlated to each other to identify voxels that were both structurally and functionally connected to similar regions within the rest of the brain. In this way, a parcellation-independent processing stream was established that makes it possible to study the relationship of structure and function within and between populations.

Furthermore, to study the impact of different methods on the results and the robustness of the approach, we compared two functional and two structural connectivity measures. Full and partial correlations were estimated to assess functional connectivity, whereas probabilistic and global fiber-tracking was performed to analyze structural connectivity. In a comparison study of different network modeling techniques (Smith et al., 2011) and in direct comparison with structural equation modeling (Marrelec et al., 2009), partial correlations performed well in reconstructing networks based on time series data. Partial correlations are commonly used to analyze direct relationships between time signals, whereas full correlations are more prone to introduce indirect connections into the model. To analyze the difference between a method focusing on direct connectivity and one that largely introduces indirect connectivity, we therefore compared estimates of partial and full correlations of functional time series in this study. To estimate structural connectivity, we used a classical, probabilistic fiber-tracking method based on a diffusion tensor model (Kreher et al., 2008) and a novel, global fiber-reconstruction technique that has been shown to perform well in the reconstruction of crossing fibers (Reisert et al., 2011). The results for the different methods were strikingly similar, revealing most parts of the default mode network, a functional network that consists of the precuneus and adjacent posterior cingulate/retrosplenial cortex (PCC/Rsp), the medial prefrontal cortex (MPFC) and inferior parietal lobes/angular gyrus (IPL/AG) as well as the medial temporal lobe (MTC). Thus, a voxel-wise comparison of structural and functional connectivity appears useful to characterize the functional and anatomical architecture of the human brain and seems to yield robust results even when using different methods.

Materials and methods

Participants

Nineteen healthy subjects (6 females, 18 right-handed) between 21 and 31 years of age (mean: 26.6, standard deviation: 2.98) participated in the study. All measurements were obtained on a 3 Tesla whole-body scanner (Trio, Siemens, Erlangen, Germany) using a birdcage radio-frequency head coil. Subjects had no neurological or psychiatric history and were not taking any psychoactive medication. The study was approved by the local ethics committee of the Charité, University Medicine Berlin and written informed consent was obtained from all subjects according to the Declaration of Helsinki.

Data acquisition

For anatomical segmentation and the construction of a group-template, high-resolution anatomical images were obtained using a standard magnetization-prepared rapid gradient-echo (MP-RAGE) sequence (TR = 1900 ms, TE = 2.52 ms, isotropic voxel-size of $1 \times 1 \times 1\,mm^3$, 192 slices).

Functional images were acquired using a gradient-echo planar imaging (EPI) sequence (TR = 2010 ms, TE = 30 ms, voxel-size $3 \times 3 \times 3\,mm^3$, 33 slices with a distance factor of 15% resulting in a slice gap of 0.45 mm covering the whole brain). During functional scanning, participants were asked to close their eyes. A total of 400 EPI volumes were acquired in two consecutive runs of about 6 min each.

Diffusion-weighted images were obtained using a diffusion-sensitive single-shot spin echo EPI sequence (TR = 10,000 ms, TE = 94 ms, voxel-size of $2 \times 2 \times 2\,mm^3$, 69 slices). An effective b-value of $1000\,s/mm^2$ was used for each of the 61 diffusion encoding directions. In addition, 9 volumes without diffusion weighting (b-value = $0\,s/mm^2$) equally distributed throughout the scan were acquired (b0-images). For both the fMRI and the diffusion weighted data, motion and distortion correction were applied during image reconstruction by using a previously acquired reference scan (Zaitsev et al., 2004).

Voxel-wise connectivity assessment

To define a consistent anatomical gray matter mask for the whole group, T1-weighted anatomical images were transformed into common space using a diffeomorphic image registration algorithm (DARTEL) as implemented in SPM8 (Ashburner, 2007; Friston et al., 2004). The gray matter volume of this template was then downsampled to obtain a total of approximately 40,000 gray matter voxels of $3.2 \times 3.2 \times 3.2\,mm^3$. This voxel-wise approach parcellates the brain without

Please cite this article as: Horn, A., et al., The structural–functional connectome and the default mode network of the human brain, NeuroImage (2013), http://dx.doi.org/10.1016/j.neuroimage.2013.09.069

implying anatomical pre-assumptions and preserves a high spatial resolution (Fig. 1). Thus, clustering of heterogeneously connected brain regions can be omitted (Rubinov and Sporns, 2010).

All connectivity measures between each pair of voxels were calculated in each participant's native subject space. To do so, all voxels obtained from the gray matter mask of the group-template were projected into both diffusion-imaging and functional single-subject spaces.

Analysis of functional images

Functional images were corrected for slice timing and rigid body movements using SPM8. Functional time series were detrended and two mean signals extracted from white matter and cerebral fluid volumes, as well as rigid body motion parameters were regressed out to minimize effects of physiological noise (Van Dijk et al., 2010; Weissenbacher et al., 2009). Signals were bandpass-filtered using a fast Fourier transformation based filter with cutoff values of 0.009 and 0.08 Hz. For each subject, approximately 40,000 (p) pre-processed time series each comprising 400 data-points (n) were obtained. In a first step, Pearson's correlation coefficients were calculated between each pair of time signals, forming a weighted, undirected connectivity matrix for each subject.

Since standard (marginal) correlations also capture indirect connectivity between two time series (e.g. if both are correlated to another time series), in a second step, functional connectivity was estimated by calculating partial correlation coefficients between all 40,000 time-series. In theory, partial correlations only describe direct connectivity between signals of a network, i.e. suppress indirect connectivity (Marrelec et al., 2006; Varoquaux and Craddock, 2013). Partial correlations can be estimated either via linear regression of time series or by estimating the inverse covariance matrix (also called the 'precision matrix') of the whole set of time series. Off-diagonal entries in this matrix can be used to calculate partial correlation coefficients directly. In a study by Smith and colleagues (Smith et al., 2011), several connectivity measures were compared and the approach that relied on estimating the inverse covariance matrix yielded best results.

However, for $n \ll p$, such an inversion of the empirical covariance matrix is an ill-posed problem, as the matrix is usually singular (Banerjee et al., 2006). Using linear optimization (http://www.di.ens.fr/~mschmidt/Software/), we therefore applied l_2-regularization on the diagonal of the matrix to make it positive definite and thus invertible. Similar approaches have been used on fMRI-data (Huang et al., 2010; Ryali et al., 2010; Varoquaux and Craddock, 2013; Varoquaux et al., 2010; Wee et al., in press) and in other domains, e.g. to analyze genetic datasets (Stifanelli et al., 2011; Witten and Tibshirani, 2009).

This procedure resulted in estimates of partial correlations between all 40,000 time series, which were used as a second functional connectivity measure. Thus, the two functional connectivity measures – full correlations and the estimates of partial correlations based on the inverse covariance matrix – resulted in two connectivity matrices for each subject. The entries x_{ij} of the two matrices estimate the full and partial correlation between the *ith* and *jth* fMRI timecourse. In the following, correlation coefficients derived from empirical correlation matrices will be referred to as 'full correlations', whereas the ones derived from the estimate of the precision matrices will be referred to as 'partial correlations'.

To prove the efficacy of the l_2-regularization approach that was applied to estimate partial correlations, network sparsity between full and partial correlation was compared, since partial correlation matrices are expected to be sparse (Banerjee et al., 2006; Smith et al., 2011). Usually, network sparsity is defined by the portion of zero-entries in a connectivity matrix. However, since in full correlations, no entries that are exactly zero exist. Sparsity was measured by the portion of connections that had absolute weights smaller than 1E-3 × standard deviation of all absolute weights within the network.

Analysis of structural images

The local diffusion parameters were calculated using the DTI & Fiber Tools for SPM (Kreher et al., 2006). As a first estimate of structural connectivity, probabilistic tracking starting from each voxel of the anatomical group-template was performed. Anatomical T1-weighted images were segmented and the resulting white matter volumes were coregistered to the b0-images to define the probabilistic tracking areas. These volumes were inflated by 5 mm to include gray matter voxels, from which probabilistic tracking was started (Umarova et al., 2010). A Monte Carlo simulation of a random walk algorithm similar to the probabilistic index of connectivity (PICo) approach was used (B. Kreher et al., 2008). Starting from each seed-voxel, the random walk was performed 10^5 times, each propagating a trajectory within the tracking area. Probability in the propagation of random walks within a certain voxel was obtained by drawing the traversed direction randomly from an orientation density function (ODF). The ODF was empirically extracted from each voxel's diffusion tensor by applying an exponent of $q = 4$ to its eigenvalues (Fletcher et al., 2007; Koch et al., 2002; B. Kreher et al., 2008).

Using this algorithm, we obtained a PICo map for every gray matter voxel on the group-template. To estimate structural connectivity between a certain pair of voxels, the PICo-value at location of the second voxel of the map that was calculated by seeding from the first and vice versa were gathered and averaged. The result formed the weight of connectivity between the pair of voxels, resulting in an undirected structural connectivity matrix for each subject. Such a voxel-wise calculation of probabilistic connectivity is computationally expensive but was possible by parallel processing over voxels on a high-performance cluster (4x32xIntel® Xeon® CPU compute cluster with 128 GB RAM) and feeding tracking results directly into the connectivity matrices. Starting from each voxel, 100,000 random-walker trajectories were propagated through the white matter of each subject. In total, this resulted in $19 \times 40{,}000 \times 100{,}000$ random-walks and an approximate computational time of 11 weeks for the whole group of subjects on 12 cores of the cluster.

As a second method to estimate structural connectivity, the Gibbs' tracking-approach (B.W. Kreher et al., 2008) supplied with the DTI & Fiber Tools for SPM (Reisert et al., 2011) was used to reconstruct the global fiber-dataset directly from the DTI volumes. Based on the raw data of the acquired high-angular diffusion imaging (HARDI) data, a piecewise approximation of neuronal pathways was achieved by annealing small cylinders to chains that finally formed fiber-tracts. These cylinders are simulated as moving particles, and their alignment to chains is attained by slowly reducing the simulated temperature of the system. In a Bayesian framework, a signal $\hat{S}^*$ is simulated by a spatially distributed sum of all cylinders and optimized iteratively during cylinder annealing to best explain the measured MR-signal $\hat{S}$. The following parameters were chosen: Starting temperature: 0.1, stop temperature: 0.001, numbers of steps: 50, numbers of iterations: 5×10^8. The "dense" parameter default value was used to estimate comparable cylinder parameters for each subject. Global tracking was performed on a tracking-mask that was obtained by segmenting the anatomical volumes and coregistering them to the b0-images.

A mean of 1.2×10^5 fibers was obtained for each subject. Fibers that left the cortex through the spinal cord were excluded, because our primary interest concerned connectivity within the cerebral cortex. Since global tracking was performed on a tracking mask that only included the white matter volume, for the evaluation of connectivity, each gray matter voxel was projected onto its closest fiber terminal if their distance did not exceed 3 mm. This was done to bridge the gap between gray and white matter and to reduce a favoring of gray matter voxels that resided close to the gray-white-matter interface (Zalesky and Fornito, 2009). For each fiber terminal, all voxels within the distance range of 3 voxels were connected with voxels within the same distance

Please cite this article as: Horn, A., et al., The structural–functional connectome and the default mode network of the human brain, NeuroImage (2013), http://dx.doi.org/10.1016/j.neuroimage.2013.09.069

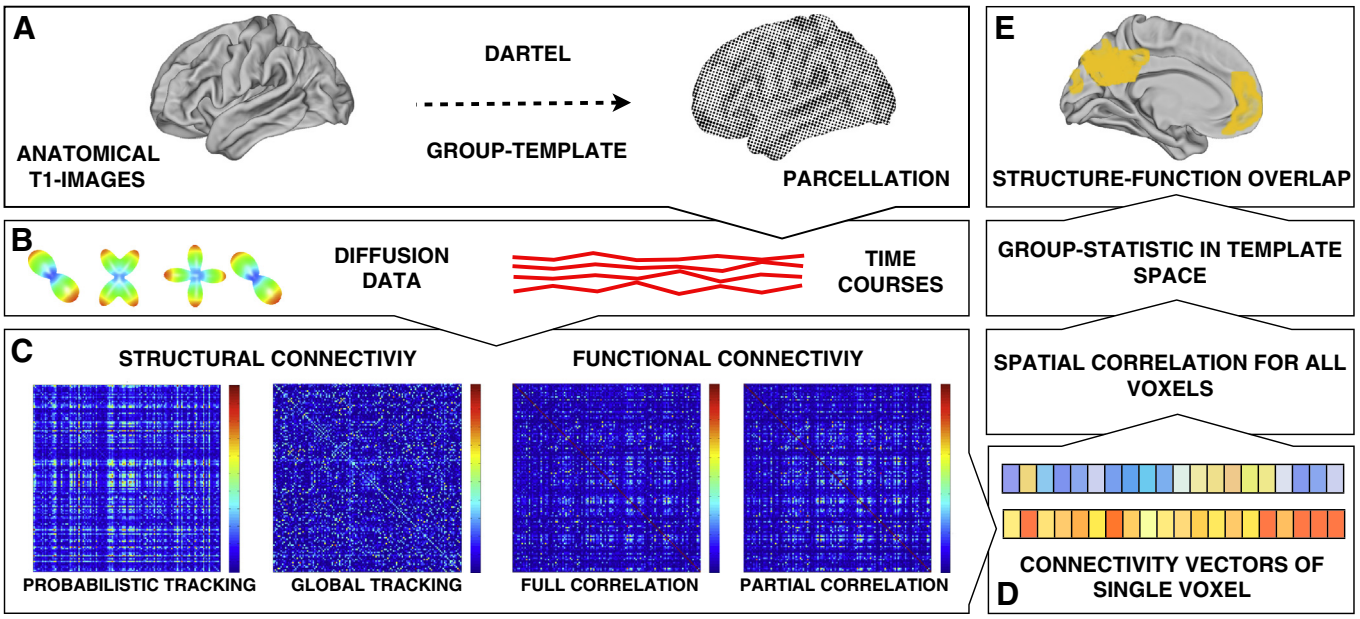

Fig. 1. Processing of functional time signals and structural data obtained from functional MRI and diffusion based imaging. Panel A: A group template as a best mean agreement between the individual anatomical features is parcellated into 40,000 voxels. Panel B: Structural and functional connectivity is obtained by using diffusion-weighted and fMRI data. Probabilistic and global tracking is performed between each point defined in panel A. Functional time courses are extracted from the same points, accordingly. Panel C: For each connectivity method, an adjacency matrix is obtained for each subject, showing the connectivity between each pair of the 40,000 voxels. Panel D: Each voxel's connectivity to the rest of the brain is represented in a $1 \times 40{,}000$ vector (i.e. one row or column extracted from the matrices in panel C). Agreement between vectors obtained from different methods within subjects can be combined by spatially correlating vectors for each voxel and by mapping resulting values back to the group-template space (panel E). Results can then be transformed to standard MNI space by applying the normalization transformation of the template to the resulting images.

range to the other end of the fiber, while connection weights were penalized linearly to distance.

In summary, two structural connectivity matrices were obtained from the two structural connectivity methods for each subject (Fig. 1). Entries x_{ij} in these matrices accounted for the number of random walks (in probabilistic tracking matrices) or number of fibers (in global tracking) that connected two voxels *i* and *j*.

Between-modality connectivity agreement

The global agreement of different connectivity analyses, i.e. the agreement of functional and structural connectivity between all voxels, was calculated by correlating two complete connectivity matrices. This procedure resulted in a single R-value for each pair of connectivity measures and each subject. Statistical significance was obtained by Fisher-transforming the R-values obtained for each subject and calculating one-sample t-tests over the group.

Since nearby voxels are more likely to be connected both in functional and structural connectivity measures (Skudlarski et al., 2008), Euclidean distance of voxels was regressed out of the connectivity vectors before correlating them to omit the introduction of false positive correlations through the effect of distance. This was done by calculating a 'distance matrix' from all voxel-coordinates, which could be used as an additional variable in a partial correlation analysis. The same analysis was performed without prior regression of Euclidean distance to show the impact of this procedure on our results.

To be able to localize regions with high agreement in their structural and functional connectivity, a spatial correlation analysis was performed (see Fig. 1). The entries x_{ij} of each of the four connectivity matrices of a subject accounted for the subject-specific connectivity between voxels *i* and *j* within the group template. Accordingly, the *i*th row of each matrix had approximately 40,000 entries that mapped the connectivity of voxel *i* to every other gray matter voxel. The structure–function agreement of that voxel could be estimated by calculating the Pearson's correlation coefficient between the *ith* row of a structural and a functional matrix (Skudlarski et al., 2008). This resulted in one Pearson's R-value for each voxel, when one row of a structural and a functional connectivity matrix were compared. A high R-value implied that the structural and functional connectivities of a certain voxel to the rest of the brain were similar. In this way, areas with high similarity in their global structural and functional connectivity could be identified (Fig. 1). This analysis assessed the distribution of similarity between connectivities across the brain.

To allow group statistics, intensity values of the spatial correlation maps were Fisher-transformed to a Gaussian distribution and z-transformed to a standard normal distribution. Spatially, images were then smoothed with an isotropic Gaussian FWHM kernel of 8 mm. Finally, one-sample t-tests were performed across subjects in a standard second-level SPM-analysis. Two-sample t-tests were used to compute differences between the connectivity measures. The main steps of the processing pipeline are summarized in Fig. 1.

Comparison with a default-mode network template

Comparison of the regions that were identified to show the highest structure–function agreement were compared to a template of the DMN obtained from a classical independent component analysis experiment (Garrity et al., 2007) as provided with the GIFT toolbox (http://mialab.mrn.org/software/gift/). Similarity was assessed by correlating intensity values of all voxels of the images with the template for each subject. High Pearson R-values imply that the resulting images were similar to the DMN template.

Global tracking from the identified regions

To obtain a structural group-connectome based on global tracking results, estimated fiber-tracts of each subject were normalized into MNI space and together formed a dataset that comprised 2.3 million fibers. The regions identified to show the highest similarity in probabilistic tracking and full correlation analyses were used as tracking seeds in this dataset. In this way, association fiber-tracts

Please cite this article as: Horn, A., et al., The structural–functional connectome and the default mode network of the human brain, NeuroImage (2013), http://dx.doi.org/10.1016/j.neuroimage.2013.09.069

that connect the identified regions to the rest of the brain could be visualized.

Results

Overall matrix agreement

Mean matrix agreement between functional and structural whole-brain connectivity matrices was assessed by calculating the Pearson's correlation coefficient between two connectivity matrices. Following the approach of (Skudlarski et al., 2008), this was done after removing the effect of Euclidean distance, i.e. by calculating the partial correlation coefficients between structural and functional connectivity matrices not accounted for by the effect of Euclidean distance. However, to be able to evaluate the impact of Euclidean distance regression, correlation values with and without prior regression of Euclidean distance are reported in Table 1.

R-values between probabilistic fiber-tracking and full correlation matrices ranged from 0.02 to 0.08 (mean: 0.046, standard-deviation 0.018) in single subjects. When comparing global fiber-trackings and full correlations of fMRI time signals, R-values ranged from 0.006 to 0.02 (mean: 0.017, standard-deviation: 0.010). Mean values of correlations decreased to 0.024 (standard-deviation 0.029) between probabilistic tracking and partial correlations and 0.015 (standard-deviation 0.017) between global tracking and partial correlations. Matrix agreement between all combinations of connectivity-measures was significant on group-level ($p < 0.001$). This shows that even in a voxel-wise comparison of connectivity, overall structural and functional connectivity are dependent on each other. The comparably low R-values may be explained by the high degree of sparsity of the structural matrices (see also discussion and Skudlarski et al., 2008) and the high amount of noise introduced by a voxel-wise comparison. As expected, within-modality comparisons resulted in higher R-values. Matrix agreement between the two functional connectivity matrices ranged between $R = 0.1$ and 0.3 (mean: 0.15, standard-deviation: 0.060). Comparison of probabilistic and global fiber-tracking yielded R-values between 0.03 and 0.18 (mean: 0.11, standard-deviation 0.064).

Since results from full and partial correlations were strikingly similar, matrix sparsities between the two measures were compared. Higher network sparsity in partial correlation connectivity matrices would confirm the assumption that the average degree of connectivity in networks derived from partial correlations is lower than in networks derived from full correlations (most likely because indirect connections are suppressed, Marrelec et al., 2009). As expected, sparsity between full and partial correlation matrices differed by two orders of magnitude in each subject (mean: 0.0007 in full correlations and 0.075 in partial correlations).

Spatial correlation of different connectivity measures

In a similar fashion, signatures of a voxel's structure–function connectivity agreement were obtained by calculating the Pearson's correlation coefficient between its functional and structural connectivity to the rest of the brain. A high R-value resulted for voxels that were connected both structurally and functionally to a similar set of other voxels in the brain. Peak correlations ranged from Pearson's R-values of 0.24 to 0.42 (mean: 0.31, standard-deviation 0.051) across subjects.

Both in single-subjects (see Fig. S1) and on a group level (see Figs. 2 and 4), agreement between functional and structural connectivity values was highest and most robust in default mode regions of the brain. The statistical group analysis of correlations between structural connectivity estimates obtained from probabilistic tracking and functional data did show strong correlations in bilateral precuneus and adjacent posterior cingulate/retrosplenial cortex (PCC/Rsp), bilateral inferior parietal lobe/angular gyrus (IPL/AG) and right supramarginal gyrus (SMG). The correlations obtained from the global tracking method revealed additional correlations within the bilateral medial prefrontal cortices (MPFC). Early visual areas were also found to show high structure–function agreement in data obtained from global trackings. Fig. 2 summarizes group-results for these findings and Fig. 4 shows the unthresholded maps of mean correlations. In Table 2, coordinates and t-values of peak voxels within the identified clusters can be found. Differences between the two tracking methods are shown in contrast images of paired t-test analyses (Fig. 3). Here, the congruence between probabilistic tracking and functional data showed higher t-values for precuneal and parietal regions, whereas the congruence between global tracking and functional data revealed higher t-values in MPFC and visual cortices.

Overall, no substantial differences were found between full and partial correlations of time signals in this analysis and group-results from the spatial correlation analyses when performed with and without prior regression of Euclidean distance were virtually identical.

Spatial comparison of the identified regions with a template of the default-mode network

Correlations of voxel-wise intensity values between the structure–function agreement maps and a template of the DMN from a functional ICA study (Garrity et al., 2007) was performed to obtain objective results about the spatial overlap between our results and the functionally defined DMN. Mean R-values ranged between 0.28 and 0.38 and are shown in Table 3 for each combination of connectivity measures. As can be seen by this analysis, the combination of probabilistic fiber-tracking and partial correlations showed regions that were most similar to the ICA-based DMN template. Here, a slight benefit of the use of partial correlations in comparison to full correlations may be seen, since regardless of the tracking algorithm applied, partial correlations yielded slightly higher R-values.

Tractography from identified regions

Global tractography from the identified regions that were found to have a high agreement between their functional and structural

Table 1
Connectivity agreement as measured by correlating whole connectivity matrices for different connectivity measures. Mean Pearson's R-values, as well as t- and p-values of a one-sample t-test over the group are given for the analyses with and without prior regression of Euclidean distance.

	Full matrix agreement with regression of Euclidean distance			Full matrix agreement without regression of Euclidean distance		
Connectivity measures	*R* (± sd)	*t*	*p*	*R* (± sd)	*t*	*p*
Full correlations/probabilistic tracking	0.046 (±0.018)	11.16	1.61E-09	0.037 (±0.018)	8.89	5.31E-08
Full correlations/global tracking	0.017 (±0.010)	7.54	5.64E-07	0.013 (±0.005)	10.80	2.68E-09
Partial correlations/probabilistic tracking	0.024 (±0.029)	8.56	9.30E-08	0.039 (±0.016)	10.49	4.23E-09
Partial correlations/global tracking	0.015 (±0.017)	8.98	4.52E-08	0.014 (±0.005)	12.79	1.80E-10
Full and partial correlations	0.148 (±0.060)	10.71	6.00E-07	0.164 (±0.064)	11.02	1.95E-09
Probabilistic and global tracking	0.111 (±0.064)	7.50	3.05E-09	0.119 (±0.036)	14.40	2.54E-11

Please cite this article as: Horn, A., et al., The structural–functional connectome and the default mode network of the human brain, NeuroImage (2013), http://dx.doi.org/10.1016/j.neuroimage.2013.09.069

connectivity to the rest of the brain revealed their widespread antero-posterior, medio-temporal and interhemispheric connectivity to other brain regions and identified the involved pathways. Specifically, the cingulum bundle promotes far-reaching antero-posterior connectivity from the retrosplenial and precuneal cortices to the medial frontal lobe and other, partly diffuse, frontal areas of the brain. Precuneal and parietal regions seem to be connected via the inferior longitudinal fascicle, which extends to the medial temporal lobe (MTL). Bihemispherical communication is largely mediated via the corpus callosum. As in (Greicius et al., 2009), we did not find direct anatomical connections between the MPFC and the MTL.

Discussion

The primary aim of this study was to introduce a method that makes it possible to investigate the structural and functional connectivity of the whole brain simultaneously. To achieve this, an observer-independent processing stream was established that computes voxel-to-voxel connectivity within the entire cerebral cortex. Two methods to estimate functional, as well as structural connectivity were compared. For all combinations of methods, areas of the default mode network showed the highest structure–function agreement within the whole brain, which is plausible with regard to recent literature (Honey et al., 2007; Skudlarski et al., 2008).

Commonly, whole-brain connectivity is investigated between regions that are based on a certain parcellation scheme (Bassett et al., 2008; Gong et al., 2009; Liu et al., 2008; Salvador et al., 2005). However, this might lead to selection bias, since the applied parcellations are typically based on preselected regions of interest (ROI) and do not account

Table 2
Results from spatial correlations between different connectivity measures. Coordinates and t-values refer to peak-voxels in significant clusters.

# in Fig. 2	Region	Peak coordinates			t
Probabilistic tracking and full correlations					
1	Bilateral Precuneus and PCC/Rsp	6	−61	34	17.12
2	Left IPL/AG	−36	−63	47	11.86
2	Right IPL/AG	45	−43	52	8.72
3	Right SMG	57	−28	25	10.45
Probabilistic tracking and partial correlations					
1	Bilateral Precuneus and PCC/Rsp	6	−58	34	16.89
2	Left IPL/AG	−54	−66	32	10.71
2	Right IPL/AG	45	−43	49	8.67
3	Right SMG	60	−28	25	11.44
Global tracking and full correlations					
1	Bilateral Precuneus and PCC/Rsp	9	−52	31	9.52
2	Left IPL/AG	−39	−46	43	10.71
2	Right IPL/AG	48	−46	28	7.97
4	Bilateral MPFC	−3	62	−8	8.28
6	Occipital cortex	−30	−100	4	10.63
Global tracking and partial correlations					
1	Bilateral Precuneus and PCC/Rsp	15	−64	32	8.72
2	Left IPL/AG	−36	−45	49	8.33
2	Right IPL/AG	39	−40	46	9.04
4	Bilateral MPFC	0	68	0	6.61
5	Left IFG	−30	50	7	6.95
6	Occipital cortex	−31	−100	8	8.79

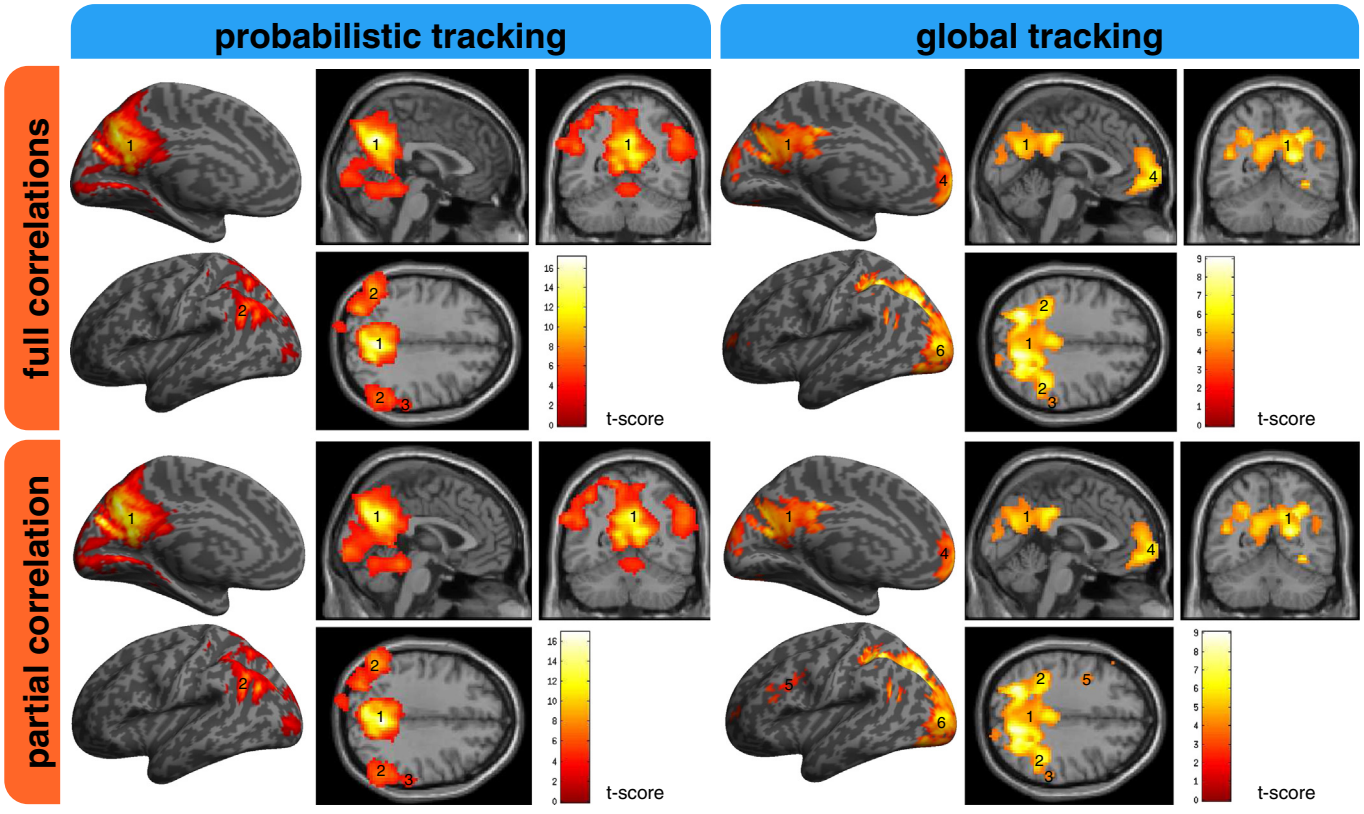

Fig. 2. Group results of correlations between functional and structural connectivity measures. Voxel-wise comparisons between each voxel's functional and structural connectivity to the rest of the brain were analyzed for each subject and analyzed in a t-test group analysis. Findings from spatial correlation analyses between one of the structural connectivity measures (probabilistic global fiber-tracking) and one of the functional connectivity measures (full or partial correlations) are shown. Areas in this figure are thresholded at $p < 0.001$ and corrected for multiple comparisons on a cluster-level (FWE < 0.05). 1: Precuneus and adjacent posterior cingulate/retrosplenial cortex (PCC/Rsp), 2. Bilateral Inferior parietal lobe/angular gyrus (IPL/AG), 3. Right Supramarginal gyrus (SMG), 4. Bilateral Medial prefrontal gyrus (MPFC), 5. Left middle/inferior frontal gyrus, 6. Occipital pole.

Please cite this article as: Horn, A., et al., The structural–functional connectome and the default mode network of the human brain, NeuroImage (2013), http://dx.doi.org/10.1016/j.neuroimage.2013.09.069

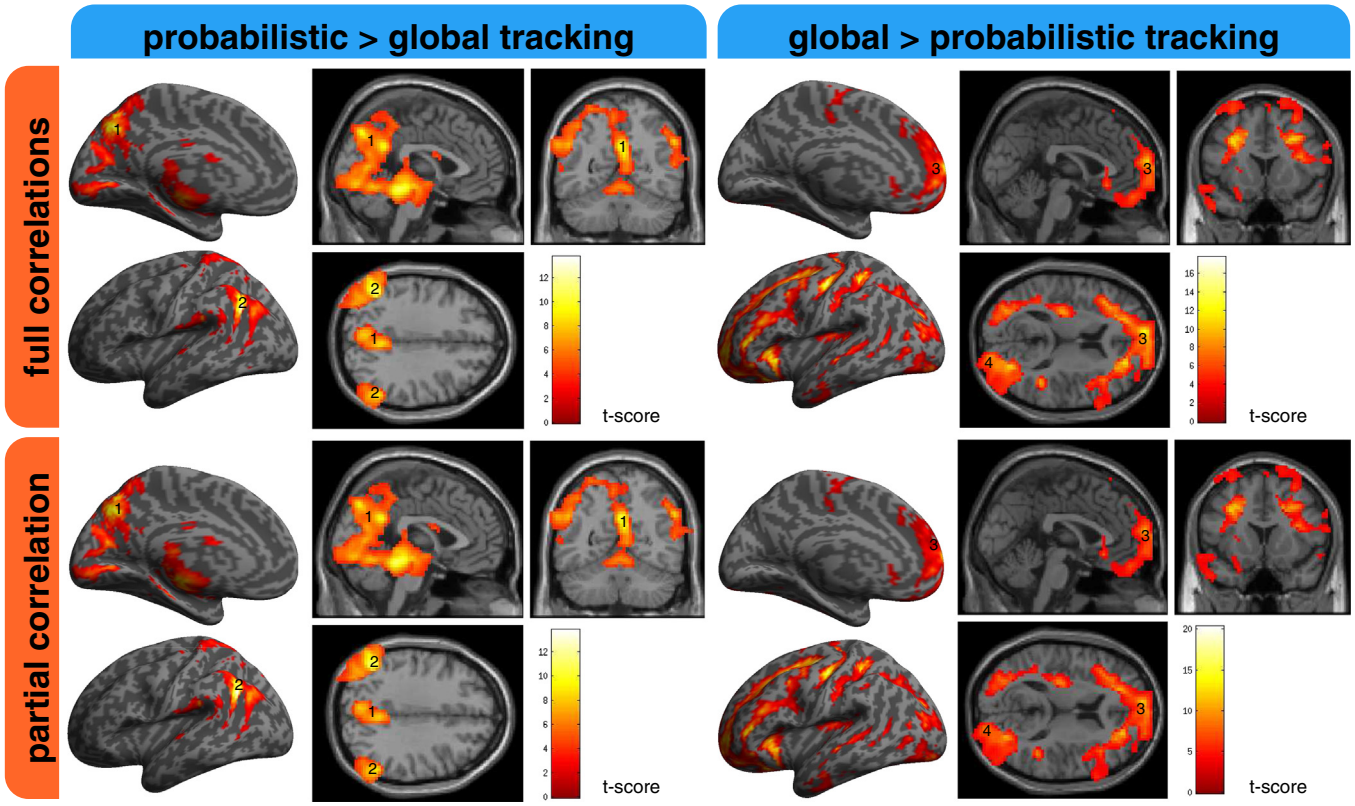

Fig. 3. Contrasts between results from Fig. 2 further show the effect of the different structural tracking methods and the similarity between functional methods. Differential contrast for probabilistic > global tracking similarity with full and partial correlations show higher t-values in the middle temporal gyrus and precuneus. Global > probabilistic tracking similarity with full and partial correlations show higher t-values in frontal areas. Areas in this figure are thresholded at $p < 0.001$ and corrected for multiple comparisons on the cluster-level (FWE < 0.05). 1: Precuneus and adjacent posterior cingulate/retrosplenial cortex (PCC/Rsp), 2. Bilateral inferior parietal lobe/angular gyrus (IPL/AG), 3. Bilateral Medial prefrontal gyrus (MPFC), 4. Occipital pole.

for inter-individual anatomical differences. This might be particularly problematic for the simultaneous analysis of functional and structural connectivity because ROI might not as a whole have a homogeneous and corresponding functional and structural connectivity architecture.

In this study, the brain connectivity was compared based on a voxel-wise estimation of structural and functional connectivity in a similar approach to (Skudlarski et al., 2008). To preserve even higher spatial resolution, the number of analyzed voxels was increased to 40,000, and to ensure inter-subject comparability between connections, voxels were defined on a group-template and projected into single-subject spaces. This way, each subject's individual anatomy was equally taken into account and an observer-independent processing stream could be established.

A challenge of voxel-wise structure–function comparisons lies in a comparably high signal noise which would be averaged out if larger regions were analyzed. Given that each matrix consisted of about 1.6 billion entries and, in the structural matrices, many of them contained (near-) zero values (Skudlarski et al., 2008), comparably low Pearson's R-values were found in a correlation analysis including the whole structural and functional connectivity matrices. In comparison to prior studies, R-values seem to decrease with the number of analyzed regions from 0.66 for 66 regions and 0.36 for 998 regions in (Honey et al., 2009; values were obtained as group-averages, leading to a second de-noising effect) to 0.18 for 5000 regions in (Skudlarski et al., 2008) and a mean of 0.03 for 40,000 regions in our study.

We applied two structural and two functional methods to analyze voxel-wise connectivity within the brain. The regions that showed the highest similarity between structural and functional connectivity differed mainly between the two tractography algorithms, whereas the functional methods yielded very similar results. The main difference between the structural methods was that probabilistic fiber-tracking did not identify the MPFC as a significant region with high structure–function agreement, whereas the global tracking approach did (Figs. 2 and 3). On the unthresholded maps of mean correlation strength over the group, however, the MPFC can be seen in analyses involving probabilistic fiber-trackings, as well (Fig. 4). Within the DMN, the MPFC is connected to precuneal and posterior cingulate regions via the cingulum bundle (Greicius et al., 2009), a thin association tract that is characterized by sharp changes in orientation. Partial volume effects caused by its propagation within the cingulate cortex make it even more difficult to reconstruct in tractography studies (Awate et al., 2007). A less robust reconstruction of this fiber-tract by the probabilistic tracking algorithm could explain the differences in our results.

It might seem more surprising, however, that partial correlations yielded only slightly different results than full correlations. Most likely, the sparsity of the structural connectivity matrices contributes to this effect, since voxels that are anatomically well connected are probably equally well connected in full and partial correlations (Greicius et al., 2009; Honey et al., 2009; Koch et al., 2002). To further analyze the similarity of the findings between full and partial correlations, we compared network sparsities of both connectivity matrices, which differed

Table 3
Intensity values in brain-maps showing regions with high cross-modal connectivity agreement were correlated to intensity values in a template of the default mode network obtained from a classical independent component analysis study (Garrity et al., 2007). Mean correlation strength of single-subject images with the template and their standard deviation are displayed for the combinations between the two functional and structural methods applied.

Pearson's R (± standard deviations) showing similarity to DMN template		
	Probabilistic fiber-tracking	Global fiber-tracking
Full correlations	0.3810 (±0.081)	0.2799 (±0.135)
Partial correlations	0.3832 (±0.081)	0.2810 (±0.135)

Please cite this article as: Horn, A., et al., The structural–functional connectome and the default mode network of the human brain, NeuroImage (2013), http://dx.doi.org/10.1016/j.neuroimage.2013.09.069

by two orders of magnitude in each subject. This suggests that the regularization approach used to estimate the partial correlation matrices was effective, since partial correlation matrices seem to contain less indirect connections. It appears, however, that indirect connections as introduced by full correlations do not drastically change the results of structure-function-agreements, most-likely because of the high number of overall connections, which might average out (false positive) indirect connectivity estimates. This is important, since the computational demand of the two techniques varies significantly. Still, one should not underestimate the additional information that can be gained from partial correlations, especially when analyzing sub-networks, e.g. in ROI-based analyses.

The regions that were identified to show the highest agreement in structural and functional connectivity were part of the default mode network (DMN), a network that shows reduced activity during tasks (Greicius and Menon, 2004) and elevated activity when subjects are at rest (Raichle et al., 2001). Anatomically, the DMN consists of the precuneus and adjacent posterior cingulate/retrosplenial cortex (PCC/Rsp), the medial prefrontal cortex (MPFC) and the inferior parietal lobe/angular gyrus (IPL/AG), as well as the lateral/medial temporal cortex (LTC) (Buckner et al., 2008). It has been shown that parts of the DMN, namely the precuneus and posterior cingulate complex, might represent a 'structural core' of the brain (Hagmann et al., 2008), since they show the highest degree of connectivity in diffusion spectrum imaging based fiber-tracking. Default mode areas also seem to play the most central role in graph-theoretical analyses of functional data acquired at rest (Achard et al., 2006; Buckner et al., 2009; Zuo et al., 2011). Tractography starting from default mode regions performed in the present and previous studies (Greicius et al., 2009) revealed their widespread antero-posterior connectivity to other regions within the brain (Fig. 5). The cingulum bundle plays a central role in connecting precuneus and MPFC. Cingular bundles have also been considered to promote connectivity to parietal regions (Greicius et al., 2009), whereas the inferior longitudinal fascicle is considered to connect the precuneus to the temporal lobe (Buckner et al., 2008). Taken together, our findings provide additional evidence that DMN regions form central and well-connected areas within the brain. In congruence with the results of (Skudlarski et al., 2008), our findings show that DMN regions also exhibit the best agreement between their overall structural and functional connectivity, which suggests that the DMN is the functional brain network that uses the most direct anatomical connections.

In agreement with the above, results from studies that simulated functional connectivity based on empirical structural connectivity have led to the hypothesis that human neuroanatomy allows for certain functional modes to be active over time (Deco et al., 2011). It has been shown that the DMN is synchronized more often and for a longer time than other functional networks, which was explained by the high degree of structural connectivity within DMN regions (Senden et al., 2012). Our findings may elaborate on this structure–function relationship of the DMN in the following way: If functional connectivity of the DMN does not only show a high overall degree of structural and functional connectivity, but also the highest overlap between their connectivity configurations, i.e. if the DMN functionally uses more direct anatomical connections than other resting state networks, it is plausible that it is more likely to be active over time. In the absence of a task, i.e. the absence of external driving sources that could modulate the functional states of brain activity, functional dynamics seems to converge in the most stable state that is fostered by brain anatomy (Honey et al., 2010; Senden et al., 2012; Sporns et al., 2000). Our findings support the hypothesis that the network that is active in such a state is the default mode network. If brain anatomy has indeed evolved in a way that naturally leads to self-referential thought and internal mentation as a 'default' cognitive process, this would cause a better exploitation of available cognitive resources. To state this differently: When cognitive capacity is not used to solve external problems, it might be most effectively (i.e. driven by anatomy) used to evaluate and monitor the current internal state (i.e. perform internal mentation, etc.).

Apart from regions within the DMN, statistical analysis showed significant agreement between structural and functional connectivity in visual cortices using the global tracking approach. Only in the analysis that combined global tracking and partial correlations, an additional cluster within the left inferior frontal gyrus was identified. Besides, regions within the cerebellum were found in statistical analyses to show high structure–function agreement in all combinations of methods. Apart from the latter, no regions that do not form part of the DMN have been found consistently across different connectivity measures and are thus not profoundly discussed. Findings in the visual cortices and cerebellum could be interpreted to result from the high overall degree of connectivity in these regions. On the unthresholded maps in Fig. 4, regions that exhibit low structure–function agreement can also be identified.

The clinical relevance of functional and structural connectivity can be seen in many studies that analyzed connectivity in schizophrenic populations (Calhoun et al., 2011; Lynall et al., 2010; Skudlarski et al., 2010; Venkataraman et al., 2012), the effects of aging (Zuo et al., 2011) or stroke (Nomura et al., 2010). However, structural and functional connectivity are often studied independently of one another. Since structural lesions have effects on the functional organization, which due to brain plasticity again shapes structural connectivity

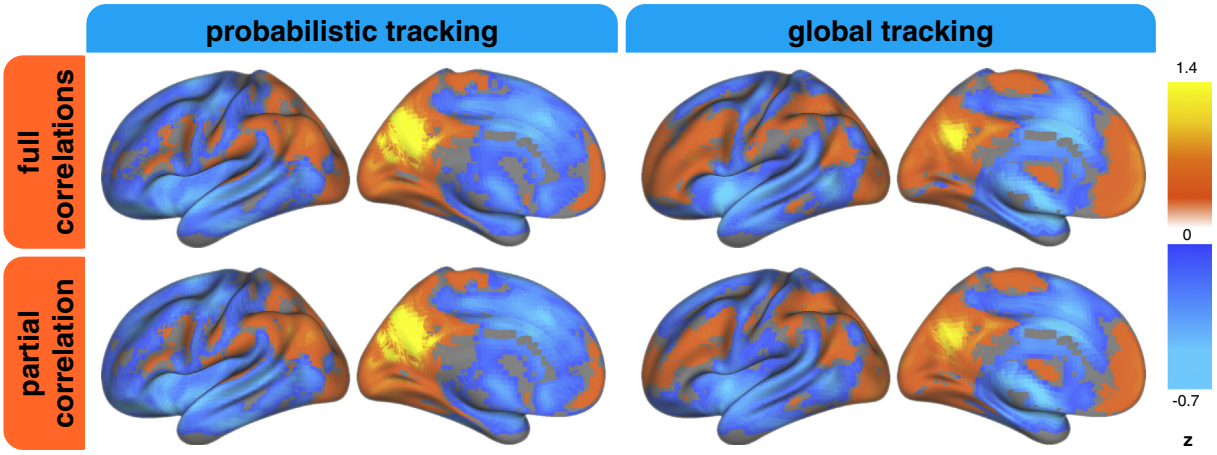

Fig. 4. Unthresholded maps of mean effect size from spatial correlation analyses for the different connectivity measures. Voxel-wise comparisons between each voxel's functional and structural connectivity to the rest of the brain were analyzed for each subject and then averaged over the group of subjects. Note that Pearson's R-values were Fisher-transformed to a gaussian distribution prior to averaging over subjects.

Please cite this article as: Horn, A., et al., The structural–functional connectome and the default mode network of the human brain, NeuroImage (2013), http://dx.doi.org/10.1016/j.neuroimage.2013.09.069

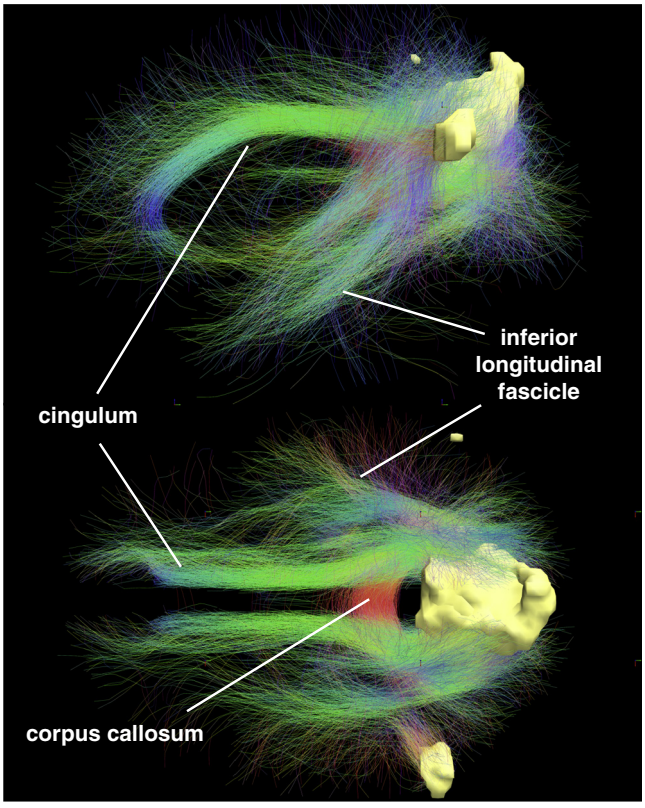

Fig. 5. Influence of the identified regions as shown by their connectivity in tractography. Regions that showed the highest structure–function agreement in between probabilistic trackings and full correlations are visualized as the solid regions in yellow. Only fibers that connect to these regions are displayed and color-coded for their traversing direction (xyz mapping to rgb). Fibers of the cingulum bundle connect precuneal regions to the medial prefrontal cortex, inferior longitudinal fascicle to the temporal lobes. Interhemispheric connectivity is mediated via the corpus callosum.

(Alstott et al., 2009), brain connectivity could be analyzed more deliberately, if structural and functional connectivity was taken into account simultaneously. The approach of this study allows for expressing a signature of a voxel's whole brain functional and structural connectivity as a single intensity value, which in analogy to methods such as voxel-based morphometry (Ashburner and Friston, 2000) enables comparisons between populations. Once differences are detected, the underlying connectivity matrices can be used to further classify them as results from structural, functional, or mixed causes. In this way, population differences could be detected and further analyzed using a voxel-wise multimodal connectivity approach.

To summarize, in this study we calculated structural and functional connectivity between each voxel within the gray matter of the brain using four connectivity methods. We were able to show that the similarity between functional and structural connectivity is highest in regions of the default mode network. This observer-independent approach may further be used to study the interplay between structure and function within and between populations.

Supplementary data to this article can be found online at http://dx.doi.org/10.1016/j.neuroimage.2013.09.069.

Acknowledgments

This work was supported by a grant from the German Federal Ministry of Education and Research (Bundesministerium für Bildung und Forschung; F.B.) and by the German Research Foundation (DFG), KFO247. We would like to thank Mark Schmidt, Ryszard Auksztulewicz and Timo Schmidt for their helpful advice.

Conflict of interest statement

We hereby certify that there is no conflict of interest regarding the material discussed in the manuscript.

References

Achard, S., Salvador, R., Whitcher, B., Suckling, J., Bullmore, E., 2006. A resilient, low-frequency, small-world human brain functional network with highly connected association cortical hubs. J. Neurosci. 26, 63–72.
Alstott, J., Breakspear, M., Hagmann, P., Cammoun, L., Sporns, O., 2009. Modeling the impact of lesions in the human brain. PLoS Comput. Biol. 5, e1000408.
Ashburner, J., 2007. A fast diffeomorphic image registration algorithm. NeuroImage 38, 95–113.
Ashburner, J., Friston, K.J., 2000. Voxel-based morphometry—the methods. NeuroImage 11, 805–821.
Awate, S.P., Zhang, H., Gee, J.C., 2007. Fuzzy nonparametric DTI segmentation for robust cingulum-tract extraction. Med Image Comput. Comput. Assist. Interv. 10, 294–301.
Banerjee, O., Ghaoui, El.L., d'Aspremont, A., Natsoulis, G., 2006. Convex optimization techniques for fitting sparse Gaussian graphical models. Presented at the ICML '06: Proceedings of the 23rd international conference on Machine learning. ACM.
Bassett, D.S., Bullmore, E.T., 2009. Human brain networks in health and disease. Curr. Opin. Neurol. 22, 340–347.
Bassett, D.S., Bullmore, E., Verchinski, B.A., Mattay, V.S., Weinberger, D.R., Meyer-Lindenberg, A., 2008. Hierarchical organization of human cortical networks in health and schizophrenia. J. Neurosci. 28, 9239–9248.
Biswal, B.B., Mennes, M., Zuo, X.-N., Gohel, S., Kelly, C., Smith, S.M., Beckmann, C.F., Adelstein, J.S., Buckner, R.L., Colcombe, S., Dogonowski, A.-M., Ernst, M., Fair, D., Hampson, M., Hoptman, M.J., Hyde, J.S., Kiviniemi, V.J., Kötter, R., Li, S.-J., Lin, C.-P., Lowe, M.J., Mackay, C., Madden, D.J., Madsen, K.H., Margulies, D.S., Mayberg, H.S., McMahon, K., Monk, C.S., Mostofsky, S.H., Nagel, B.J., Pekar, J.J., Peltier, S.J., Petersen, S.E., Riedl, V., Rombouts, S.A.R.B., Rypma, B., Schlaggar, B.L., Schmidt, S., Seidler, R.D., Siegle, G.J., Sorg, C., Teng, G.-J., Veijola, J., Villringer, A., Walter, M., Wang, L., Weng, X.-C., Whitfield-Gabrieli, S., Williamson, P., Windischberger, C., Zang, Y.-F., Zhang, H.-Y., Castellanos, F.X., Milham, M.P., 2010. Toward discovery science of human brain function. Proc. Natl. Acad. Sci. 107, 4734–4739.
Buckner, R.L., Andrews-Hanna, J.R., Schacter, D.L., 2008. The brain's default network: anatomy, function, and relevance to disease. Ann. N. Y. Acad. Sci. 1124, 1–38.
Buckner, R.L., Sepulcre, J., Talukdar, T., Krienen, F.M., Liu, H., Hedden, T., Andrews-Hanna, J.R., Sperling, R.A., Johnson, K.A., 2009. Cortical hubs revealed by intrinsic functional connectivity: mapping, assessment of stability, and relation to Alzheimer's disease. J. Neurosci. 29, 1860–1873.
Calhoun, V.D., Sui, J., Kiehl, K., Turner, J., Allen, E., Pearlson, G., 2011. Exploring the psychosis functional connectome: aberrant intrinsic networks in schizophrenia and bipolar disorder. Front. Psychiatry 2, 75.
Damoiseaux, J.S., Greicius, M.D., 2009. Greater than the sum of its parts: a review of studies combining structural connectivity and resting-state functional connectivity. Brain Struct. Funct. 213, 525–533.
Deco, G., Jirsa, V.K., McIntosh, A.R., 2011. Emerging concepts for the dynamical organization of resting-state activity in the brain. Nat. Rev. Neurosci. 12, 43–56.
Fischl, B., van der Kouwe, A., Destrieux, C., Halgren, E., Ségonne, F., Salat, D.H., Busa, E., Seidman, L.J., Goldstein, J., Kennedy, D., Caviness, V., Makris, N., Rosen, B., Dale, A.M., 2004. Automatically parcellating the human cerebral cortex. Cereb. Cortex 14, 11–22.
Fletcher, P.T., Tao, R., Jeong, W.-K., Whitaker, R.T., 2007. A volumetric approach to quantifying region-to-region white matter connectivity in diffusion tensor MRI. Inf. Process. Med. Imaging 20, 346–358.
Friston, K.J., Holmes, A.P., Worsley, K.J., Poline, J.P., Frith, C.D., Frackowiak, R.S.J., 2004. Statistical parametric maps in functional imaging: a general linear approach. Hum. Brain Mapp. 2, 189–210.
Garrity, A.G., Pearlson, G.D., McKiernan, K., Lloyd, D., Kiehl, K.A., Calhoun, V.D., 2007. Aberrant "default mode" functional connectivity in schizophrenia. Am. J. Psychiatry 164, 450–457.
Gong, G., He, Y., Concha, L., Lebel, C., Gross, D.W., Evans, A.C., Beaulieu, C., 2009. Mapping anatomical connectivity patterns of human cerebral cortex using in vivo diffusion tensor imaging tractography. Cereb. Cortex 19, 524–536.
Greicius, M.D., Menon, V., 2004. Default-mode activity during a passive sensory task: uncoupled from deactivation but impacting activation. J. Cogn. Neurosci. 16, 1484–1492.
Greicius, M.D., Supekar, K., Menon, V., Dougherty, R.F., 2009. Resting-state functional connectivity reflects structural connectivity in the default mode network. Cereb. Cortex 19, 72–78.
Hagmann, P., Cammoun, L., Gigandet, X., Meuli, R., Honey, C.J., Wedeen, V.J., Sporns, O., 2008. Mapping the structural core of human cerebral cortex. PLoS Biol. 6, e159.
Honey, C.J., Kötter, R., Breakspear, M., Sporns, O., 2007. Network structure of cerebral cortex shapes functional connectivity on multiple time scales. Proc. Natl. Acad. Sci. U. S. A. 104, 10240–10245.
Honey, C.J., Sporns, O., Cammoun, L., Gigandet, X., Thiran, J.P., Meuli, R., Hagmann, P., 2009. Predicting human resting-state functional connectivity from structural connectivity. Proc. Natl. Acad. Sci. 106, 2035–2040.
Honey, C.J., Thivierge, J.-P., Sporns, O., 2010. Can structure predict function in the human brain? NeuroImage 52, 766–776.
Huang, S., Li, J., Sun, L., Ye, J., Fleisher, A., Wu, T., Chen, K., Reiman, E., 2010. Learning brain connectivity of Alzheimer's disease by sparse inverse covariance estimation. NeuroImage 50, 935–949.

Please cite this article as: Horn, A., et al., The structural–functional connectome and the default mode network of the human brain, NeuroImage (2013), http://dx.doi.org/10.1016/j.neuroimage.2013.09.069

Koch, M.A., Norris, D.G., Hund-Georgiadis, M., 2002. An investigation of functional and anatomical connectivity using magnetic resonance imaging. NeuroImage 16, 241–250.
Kreher, B., Hennig, J., Il'yasov, K., 2006. DTI-fibertools: a complete toolbox for DTI calculation, fiber tracking, and combined evaluation. Proceedings of the 14th Annual Meeting ISMRM.
Kreher, B., Schnell, S., Mader, I., Il'yasov, K., Hennig, J., Kiselev, V.G., Saur, D., 2008a. Connecting and merging fibres: pathway extraction by combining probability maps. NeuroImage 1–9.
Kreher, B.W., Mader, I., Kiselev, V.G., 2008b. Gibbs tracking: a novel approach for the reconstruction of neuronal pathways. Magn. Reson. Med. 60, 953–963.
Liu, Y., Liang, M., Zhou, Y., He, Y., Hao, Y., Song, M., Yu, C., Liu, H., Liu, Z., Jiang, T., 2008. Disrupted small-world networks in schizophrenia. Brain 131, 945–961.
Lynall, M.-E., Bassett, D.S., Kerwin, R., McKenna, P.J., Kitzbichler, M., Muller, U., Bullmore, E., 2010. Functional connectivity and brain networks in schizophrenia. J. Neurosci. 30, 9477–9487.
Marrelec, G., Krainik, A., Duffau, H., Pélégrini-Issac, M., Lehéricy, S., Doyon, J., Benali, H., 2006. Partial correlation for functional brain interactivity investigation in functional MRI. NeuroImage 32, 228–237.
Marrelec, G., Kim, J., Doyon, J., Horwitz, B., 2009. Large-scale neural model validation of partial correlation analysis for effective connectivity investigation in functional MRI. Hum. Brain Mapp. 30, 941–950.
Nomura, E.M., Gratton, C., Visser, R.M., Kayser, A., Perez, F., D'Esposito, M., 2010. Double dissociation of two cognitive control networks in patients with focal brain lesions. Proc. Natl. Acad. Sci. 107, 12017–12022.
Raichle, M.E., MacLeod, A.M., Snyder, A.Z., Powers, W.J., Gusnard, D.A., Shulman, G.L., 2001. A default mode of brain function. Proc. Natl. Acad. Sci. U. S. A. 98, 676–682.
Reisert, M., Mader, I., Anastasopoulos, C., Weigel, M., Schnell, S., Kiselev, V., 2011. Global fiber reconstruction becomes practical. NeuroImage 54, 955–962.
Rubinov, M., Sporns, O., 2010. Complex network measures of brain connectivity: uses and interpretations. NeuroImage 52, 1059–1069.
Ryali, S., Supekar, K., Abrams, D.A., Menon, V., 2010. Sparse logistic regression for whole-brain classification of fMRI data. NeuroImage 51, 13.
Rykhlevskaia, E., Gratton, G., Fabiani, M., 2008. Combining structural and functional neuroimaging data for studying brain connectivity: a review. Psychophysiology 45, 173–187.
Salvador, R., Suckling, J., Coleman, M.R., Pickard, J.D., Menon, D., Bullmore, E., 2005. Neurophysiological architecture of functional magnetic resonance images of human brain. Cereb. Cortex 15, 1332–1342.
Segall, J.M., Allen, E.A., Jung, R.E., Erhardt, E.B., Arja, S.K., Kiehl, K., Calhoun, V.D., 2012. Correspondence between structure and function in the human brain at rest. Front. Neuroinform. 6, 10.
Senden, M., Goebel, R., Deco, G., 2012. Structural connectivity allows for multi-threading during rest: the structure of the cortex leads to efficient alternation between resting state exploratory behavior and default mode processing. NeuroImage 60, 2274–2284.
Shulman, G.L., Fiez, J.A., Corbetta, M., Buckner, R.L., Miezin, F.M., Raichle, M.E., Petersen, S.E., 1997. Common Blood Flow Changes across Visual Tasks: 11. Decreases in Cerebral Cortex. J. Cogn. Neurosci. 9, 648–663.
Skudlarski, P., Jagannathan, K., Calhoun, V.D., Hampson, M., Skudlarska, B.A., Pearlson, G., 2008. Measuring brain connectivity: diffusion tensor imaging validates resting state temporal correlations. NeuroImage 43, 554–561.
Skudlarski, P., Jagannathan, K., Anderson, K., Stevens, M.C., Calhoun, V.D., Skudlarska, B.A., Pearlson, G., 2010. Brain connectivity is not only lower but different in schizophrenia: a combined anatomical and functional approach. Biol. Psychiatry 68, 61–69.
Smith, S.M., Miller, K.L., Salimi-Khorshidi, G., Webster, M., Beckmann, C.F., Nichols, T.E., Ramsey, J.D., Woolrich, M.W., 2011. Network modelling methods for FMRI. NeuroImage 54, 875–891.
Sporns, O., 2011. The human connectome: a complex network. Ann. N. Y. Acad. Sci. 1224, 109–125.
Sporns, O., Tononi, G., Edelman, G.M., 2000. Theoretical neuroanatomy: relating anatomical and functional connectivity in graphs and cortical connection matrices. Cereb. Cortex 10, 127–141.
Sporns, O., Tononi, G., Kötter, R., 2005. The human connectome: a structural description of the human brain. PLoS Comput. Biol. 1, e42.
Stifanelli, P.F., Creanza, T.M., Anglani, R., Liuzzi, V.C., Mukherjee, S., Ancona, N., 2011. A comparative study of Gaussian graphical model approaches for genomic data (arXiv).
Umarova, R.M., Saur, D., Schnell, S., Kaller, C.P., Vry, M.-S., Glauche, V., Rijntjes, M., Hennig, J., Kiselev, V., Weiller, C., 2010. Structural connectivity for visuospatial attention: significance of ventral pathways. Cereb. Cortex 20, 121–129.
van den Heuvel, M., Mandl, R., Luigjes, J., Pol, H.H., 2008. Microstructural organization of the cingulum tract and the level of default mode functional connectivity. J. Neurosci. 28, 10844–10851.
Van Dijk, K.R.A., Hedden, T., Venkataraman, A., Evans, K.C., Lazar, S.W., Buckner, R.L., 2010. Intrinsic functional connectivity as a tool for human connectomics: theory, properties, and optimization. J. Neurophysiol. 103, 297–321.
Varoquaux, G., Craddock, R.C., 2013. Learning and comparing functional connectomes across subjects. NeuroImage 1–14.
Varoquaux, G., Gramfort, A., Poline, J.-B., Thirion, B., 2010. Brain covariance selection: better individual functional connectivity models using population prior. NIPS.
Venkataraman, A., Whitford, T.J., Westin, C.-F., Golland, P., Kubicki, M., 2012. Whole brain resting state functional connectivity abnormalities in schizophrenia. Schizophr. Res. 139, 7–12.
Wee, C.-Y., Yap, P.-T., Zhang, D., Wang, L., Shen, D., 2013. Group-constrained sparse fMRI connectivity modeling for mild cognitive impairment identification. Brain Struct. Funct. (in press).
Weissenbacher, A., Kasess, C., Gerstl, F., Lanzenberger, R., Moser, E., Windischberger, C., 2009. Correlations and anticorrelations in resting-state functional connectivity MRI: a quantitative comparison of preprocessing strategies. NeuroImage 47, 1408–1416.
Witten, D.M., Tibshirani, R., 2009. Covariance-regularized regression and classification for high-dimensional problems. J. R. Stat. Soc. Series B Stat. Methodol. 71, 615–636.
Xu, L., Pearlson, G., Calhoun, V.D., 2009. Joint source based morphometry identifies linked gray and white matter group differences. NeuroImage 44, 777–789.
Zaitsev, M., Hennig, J., Speck, O., 2004. Point spread function mapping with parallel imaging techniques and high acceleration factors: fast, robust, and flexible method for echo-planar imaging distortion correction. Magn. Reson. Med. 52, 1156–1166.
Zalesky, A., Fornito, A., 2009. A DTI-derived measure of cortico-cortical connectivity. IEEE Trans. Med. Imaging 28, 1023–1036.
Zuo, X.-N., Ehmke, R., Mennes, M., Imperati, D., Castellanos, F.X., Sporns, O., Milham, M.P., 2011. Network centrality in the human functional connectome. Cereb. Cortex 22, 1862–1875.

Please cite this article as: Horn, A., et al., The structural–functional connectome and the default mode network of the human brain, NeuroImage (2013), http://dx.doi.org/10.1016/j.neuroimage.2013.09.069